Vanadium Redox Flow Batteries

Ruiyong Chen[1], *Zhifeng Huang*[1], *Rolf Hempelmann*[1], *Dirk Henkensmeier*[2], *and Sangwon Kim*[3]

[1] *Saarland University, Saarbrücken, Germany*
[2] *Korea Institute of Science and Technology (KIST), Seoul, Republic of Korea*
[3] *KIST Europe, Saarbrücken, Germany*

1 Introduction

With a continuous decrease of the cost in the utilization of intermittent renewable energy sources such as wind and solar power in the recent years, low-cost and high-performance energy storage systems for peak-shaving and load-leveling in smart grid networks are urgently needed. As one of the most promising stationary energy storage systems, vanadium redox flow batteries (RFBs) have been first developed in the 1980s by Skyllas-Kazacos and co-workers [1–5]. Although current vanadium RFBs still have a relatively low volumetric energy density ($\sim$30 Wh l^{-1}), and a two to five times higher capital cost than the US Department of Energy's target cost of \$100 kWh^{-1} for deep market penetration, vanadium RFBs have been widely investigated and are recognized as one of the most reliable systems among the known RFB electrolyte chemistries [6–10]. The inevitable crossover issue for RFBs will contaminate the electrolytes. However, this can be easily handled in the all-vanadium RFBs by a simple rebalancing operation for the catholyte and anolyte. Studies mostly focus on the optimization of the electrolyte formulation, electrode materials, ion exchange membranes, flow field and stack design [11] and simulation [12–15].

Unlike some rechargeable batteries using flammable organic solvents as electrolyte components (such as the lithium-ion batteries, which have a risk of fire or explosion), the acidic aqueous vanadium electrolytes used in vanadium RFBs appear to be much safer for practical operation. In addition, the unique character of decoupled energy storage and power output for flow batteries enables a safe and cost-effective upscaling to large energy storage systems (Figure 1). The energy density (Wh) depends on the volume of electrolyte (i.e. tank size), and the concentration of active vanadium species (i.e. the total capacity), and the number of single cells of the stack (i.e. the total voltage), whereas the power (W) can be tailored by controlling the size of the cell (i.e. the deliverable current). The current commercial demonstrations for vanadium RFBs, ranging from a few kWh to

Encyclopedia of Electrochemistry: Batteries. Edited by Stefano Passerini, Dominic Bresser, Arianna Moretti, and Alberto Varzi.
Copyright © 2020 Wiley-VCH Verlag GmbH & Co. KGaA. All rights reserved.
DOI: 10.1002/9783527610426.bard110010

800 MWh scale, have been reported [16]. Further optimization in the key components of vanadium RFBs is required, including a decrease of the manufacturing cost of vanadium electrolytes [17], a higher vanadium concentration, a decrease in the electrochemical polarization and ohmic losses, and an improvement in the transport properties and reaction kinetics, which can lead to a decrease of the overall system cost, accelerating their industrialization [18].

Dissolved vanadium ions exist in four different oxidation states (VO_2^+, VO^{2+}, V^{3+} and V^{2+}) in acidic aqueous solutions. Each state has its own distinct color. The reversible conversion between chemical and electrical energy is realized by the following electrochemical reactions of vanadium species during charge (→) and discharge (←), as shown in Eqs. (1)–(3).

$$\text{Catholyte}: VO^{2+} + H_2O \leftrightarrow VO_2^+ + 2H^+ + e^-, E^0 = 1.0\,\text{V vs. SHE} \quad (1)$$

$$\text{Anolyte}: V^{3+} + e^- \leftrightarrow V^{2+}, E^0 = -0.26\,\text{V vs. SHE} \quad (2)$$

$$\text{Overall}: VO^{2+} + V^{3+} + H_2O \leftrightarrow VO_2^+ + V^{2+} + 2H^+ \quad (3)$$

V^{2+} ions are easily oxidized in air. Thus, oxygen-free conditions need to be kept for the anolyte during operation. Furthermore, the chemical and thermal stability of different vanadium ion solutions limits their optimal concentrations, and accordingly the volumetric capacity. The membranes and electrodes play a critical role for the species transport, and the reaction sites, respectively. In the following, the features of the key components of vanadium RFBs, including electrolytes, membranes and electrode materials, various measurement and characterization methods and approaches for the optimization of the performance will be discussed.

2 Vanadium Electrolytes

2.1 Synthesis of Vanadium Electrolytes

As one of the most important components of vanadium RFBs, the electrolyte has a significant impact on the operating temperature range, energy density, and capital costs. To prevent possible generation of chlorine gas, electrolytes are preferably based on sulfuric acid, not on HCl. Vanadium solutions can be prepared by using chemical or electrochemical methods with V_2O_5 as starting materials (Figure 2a) [19, 20]:

$$\text{chemical reduction of } V_2O_5: V_2O_5 + (COOH)_2 + 4H^+ \rightarrow 2VO^{2+} + 2CO_2 + 3H_2O \quad (4)$$

$$\text{electrolysis reaction}: V_2O_5 + 8H^+ + 3e^- \rightarrow V^{3+} + VO^{2+} + 4H_2O \quad (5)$$

$VOSO_4$ can also be used as starting material, which can be dissolved into H_2SO_4, forming VO^{2+} (Figure 2a). Subsequent electrochemical formulation steps are required to convert these initially obtained VO^{2+} and $V^{3.5+}$ (i.e. V^{3+} and VO^{2+} with 1 : 1 ratio) into the redox pairs of VO_2^+/V^{2+} and VO^{2+}/V^{3+}.

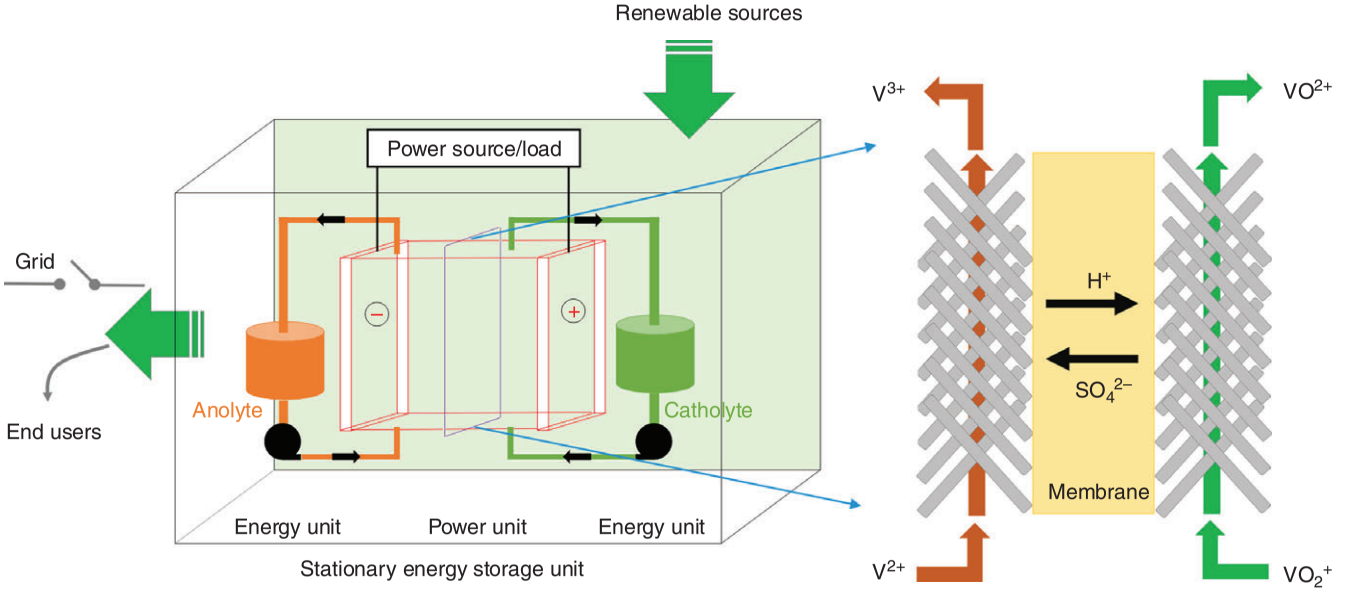

Figure 1 Schematic diagram of vanadium RFBs composed of electrochemical systems (as also depicted in the right panel), external electrolyte tanks and pumps for the utilization of renewable energy sources and the stabilization of the grid.

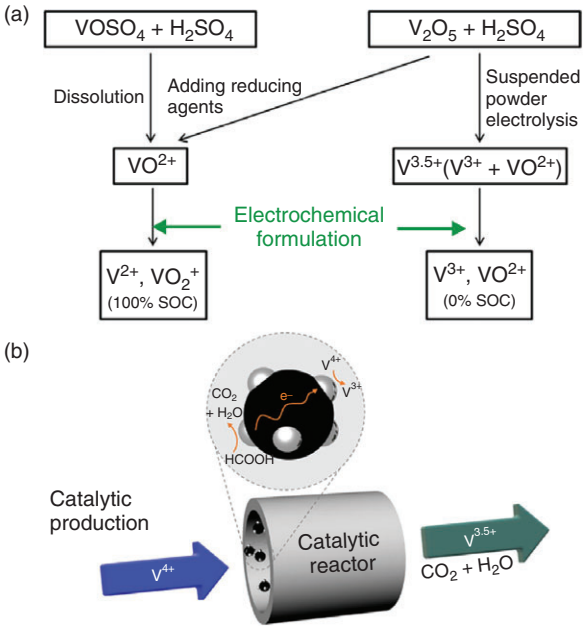

Figure 2 (a) Conventional chemical and electrochemical synthesis of vanadium electrolytes. Source: Choi et al. [19]. Reproduced with permission of Springer Nature. (b) A new catalytic production route of $V^{3.5+}$ electrolyte. Source: Heo et al. [17]. Reproduced with permission of Elsevier.

As an alternative to the costly electrolysis method, a chemical production method has been recently developed in which the chemically produced VO^{2+} is further reduced by using formic acid in a continuous catalytic reactor with Pt/C as catalyst (Figure 2b) [17].

2.2 Concentration and Chemical Stability of Vanadium Electrolytes

Since the specific energy density is proportional to the concentration of vanadium species, efforts have been made to maximize the vanadium concentration. However, the four vanadium species (VO_2^+, VO^{2+}, V^{3+} and V^{2+}) show different solubility, chemical and temperature stability at various sulfuric acid concentrations and at different temperatures [20]. Accordingly, the electrolyte temperature should be controlled and monitored during operation. These restrictions result in a compromised concentration of 1.6 M vanadium in 2 M H_2SO_4, which is often used currently as a bench-mark for commercial applications. During charge/discharge operation, the depth of the charge also affects the stability of the vanadium electrolytes, as will be discussed in Section 2.6.

Table 1 lists the thermal stability of the vanadium solutions at a broad temperature range from −35 to 50 °C [21–24]. Between 10 and 35 °C, all vanadium solutions exhibit excellent thermal stability, without the formation of any precipitates over a long measure time. Nevertheless, with a decrease in the temperature, the solutions become unstable. For instance, at −5 °C, VO^{2+} forms a precipitate

Table 1 Thermal stability of various vanadium containing solutions as a function of the concentrations of the vanadium ions and sulfate.

	Vanadium concentration (M)	Sulfate concentration (M)	*T* (°C)	Time for precipitation	Reference
V^{2+}	1.5	3.875	−35	<1 h	[21]
	1.5	3.875	−20	>2 d	[21]
	2.0	5.0	−5	>10 d	[22]
V^{3+}	1.5	3.875	−35	<1 h	[21]
	1.5	3.875	−20	>2 d	[21]
	2.0	5.0	−5	>10 d	[22]
VO^{2+}	2.0	5.0	−5	18 h	[22]
	2.0	5.0	25	95 h	[22]
	2.0	5.0	40	>33 d	[23]
VO_2^+	2.0	5.0	−5	>10 d	[22]
	2.0	5.0	25	>33 d	[23]
	1.5	4.3	40	>30 d	[24]
	2.0	5.0	40	<48 h	[24]
	3.4	6.0	40	>30 d	[24]
	5.4	7.0	40	>60 d	[24]
	2.0	5.0	50	<18 h	[23]

after 18 hours. On the other hand, by increasing the temperature above 40 °C, VO_2^+ catholytes may form V_2O_5. For 2 M VO_2^+ in 5 M sulfate solution, precipitates were observed after only two days at 40 °C [24]. At 50 °C, the precipitation time further shortened to less than seven hours [21, 23].

As studied by Skyllas-Kazacos and co-workers [25], the VO_2^+ species exists as $[VO_2(H_2O)_3]^+$ cations in the sulfuric acid solution. The hydrated ions suffer from a deprotonation process and produce a neutral species of $VO(OH)_3$ at elevated temperatures, which will irreversibly convert into insoluble V_2O_5 [24–27], as described in Eqs. (6)–(8):

$$[VO_2(H_2O)_3]^+ \rightarrow VO(OH)_3 + H_3O^+ \tag{6}$$

$$2VO(OH)_3 \rightarrow V_2O_5 + 3H_2O \tag{7}$$

$$\text{Overall}: 2VO_2^+\,(aq) + H_2O \rightarrow V_2O_5\,(s) + 2H^+\,(aq) \tag{8}$$

By increasing the temperature from 10 to 60 °C, as illustrated in Figure 3, the solubility of VSO_4, $V_2(SO_4)_3$ and $VOSO_4$ increases largely [28]. At 60 °C, the solubility of those vanadium ions can reach up to 3 M. Nevertheless, the concentration of vanadium electrolyte is limited due to the aforementioned precipitation phenomenon of VO_2^+ catholyte at temperatures above 40 °C, since the anolyte and catholyte are operated at the same temperature.

Rahman and Skyllas-Kazacos [29] evidenced that the thermal stability of VO_2^+ can be enhanced by increasing the sulfuric acid concentration. An increase in

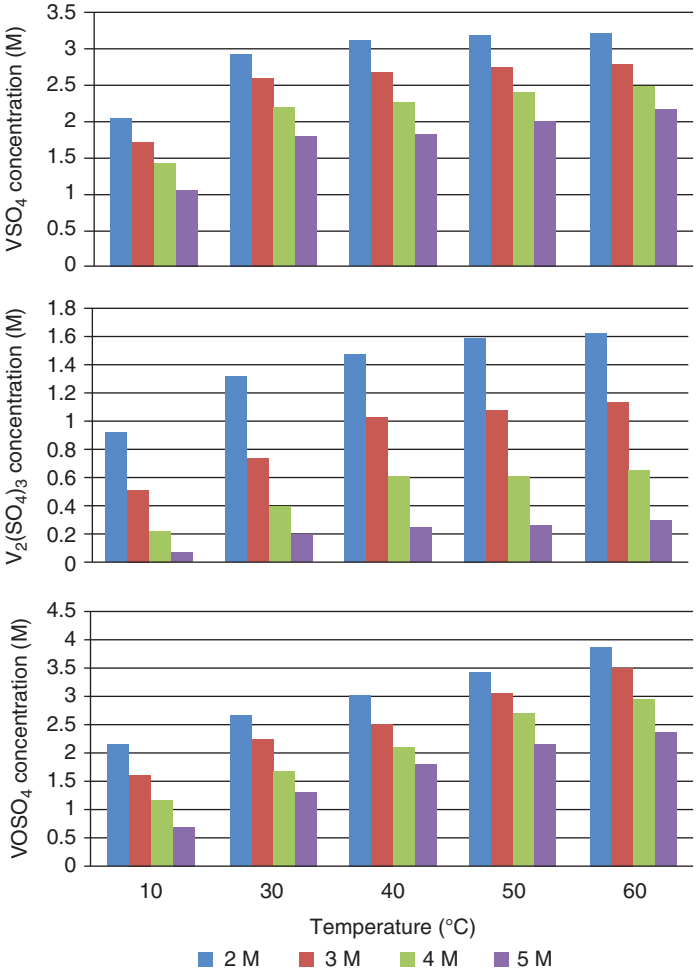

Figure 3 Solubility of VSO_4, $V_2(SO_4)_3$, and $VOSO_4$ salts as a function of temperature and initial sulfuric acid concentration. Source: Cao et al. [28]. Reproduced with permission of Multidisciplinary Digital Publishing Institute.

the proton concentration will shift the equilibrium reaction of Eq. (6) toward the left side. This will prevent the process of de-protonation or dimerization reactions. VO_2^+ concentrations as high as 5.4 M can be obtained at 40 °C when the concentration of sulfuric acid is above 5 M, as compared to a maximum VO_2^+ concentration of 2 M when the concentration of sulfuric acid is below 5 M [24, 29]. In addition, a high sulfuric acid concentration may lead to a high ionic conductivity of the electrolytes. However, the solubility of V^{2+}, V^{3+} and VO^{2+} ions decreases at higher acid concentrations, because an increase in the sulfate ion concentration will shift the equilibrium reactions to the left side, as shown in Eqs. (9)–(11), and reduce the degree of dissociation of vanadium sulfates.

$$VOSO_4 \leftrightarrow VO^{2+} + SO_4^{2-} \tag{9}$$

$$V_2(SO_4)_3 \leftrightarrow 2V^{3+} + 3SO_4{}^{2-} \tag{10}$$

$$VSO_4 \leftrightarrow V^{2+} + SO_4{}^{2-} \tag{11}$$

For instance, at 20 °C, the solubility of $VOSO_4$ decreases significantly to 0.26 M in 9 M H_2SO_4, in contrast to a solubility of 1.79 M in 3 M H_2SO_4 [30]. A similar decreasing tendency of V^{3+} ions was also observed at 30 °C [31]. With the medium concentration of 1.5 M vanadium ions (V^{2+}, V^{3+}, VO^{2+} and $VO_2{}^+$) in 3–3.5 M H_2SO_4, the optimal vanadium electrolyte composition is reached for the vanadium RFBs [32].

2.3 Ionic Conductivity and Viscosity of Electrolyte

The electrolyte conductivity plays a significant role in the mass transport and the ohmic resistance. It was found that the ionic conductivity of vanadium electrolytes is related to the state-of-charge (SOC) and the temperature [21, 33]. The ionic conductivity for V^{2+}, V^{3+} and V^{4+} ions showed an obvious increase with rising temperature. Moreover, the conductivity of the electrolyte increases with the concentration of sulfate and chlorine ions, but decreases with the concentration of vanadium ions [21, 29, 34]. At a given concentration of sulfate electrolyte, an increase in the $VO_2{}^+$ concentration will lower the free H_2SO_4 concentration in the solution, resulting in a decrease in the conductivity [35, 36]. For instance, in concentrated sulfuric acid solutions (5–7 M), the conductivity decreases by about 70% when the $VO_2{}^+$ ion concentration increases from 2 to 5 M, as shown in Figure 4a [29].

The viscosity of the electrolytes affects the distribution of the redox electrolyte in the reaction area and the energy consumption of the pump. An increase in the vanadium concentration will lead to an increase in viscosity because of the increased intermolecular interactions, and dimerization of some vanadium ions. At elevated temperatures, the decrease in the molecular interactions facilitates the transport of species. As shown in Figure 4b, the viscosity drops rapidly when the temperature increases from −20 to 50 °C [21]. The V^{3+} electrolyte exhibits the highest viscosity due to its lowest diffusion coefficient, according to the Stokes–Einstein equation, Eq. (12):

$$D = \frac{k_B T}{\eta} \tag{12}$$

where D is the diffusion coefficient, k_B is the Boltzmann constant, T is the temperature and η is the viscosity.

2.4 Mixed-Acid Vanadium Electrolytes

Noticeably, it is an effective strategy to improve the thermal stability and solubility of vanadium ions by simply tailoring the composition of the supporting electrolytes. Skyllas-Kazacos [37] has reported that 4 M V^{2+} and V^{3+} solutions can be prepared in pure hydrochloric acid supporting electrolytes. A 3 M $VO_2{}^+$ solution showed a superior stability in the chloride solution in comparison to

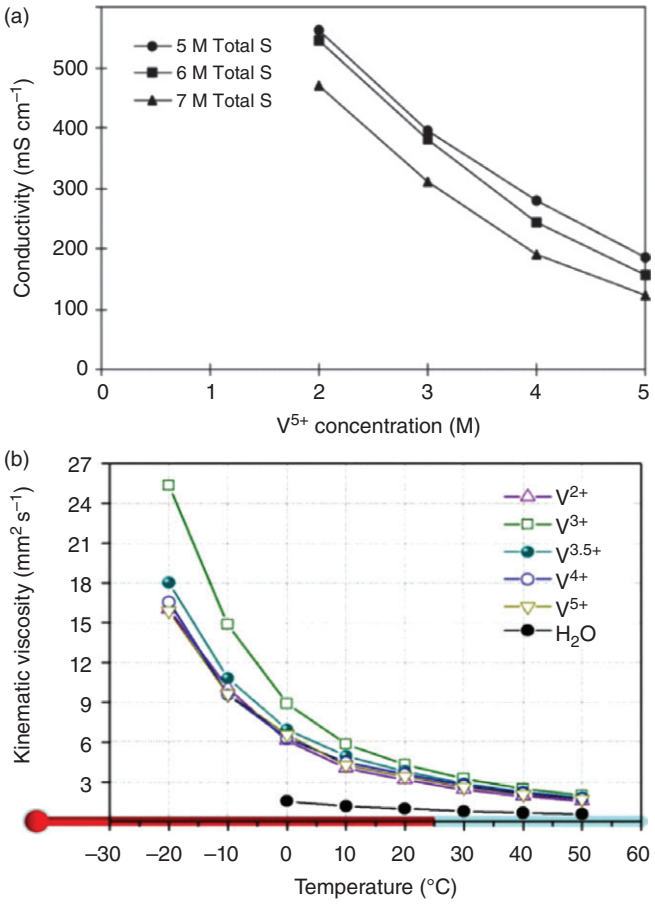

Figure 4 (a) Ionic conductivity of VO_2^+ in sulfuric acid of different concentrations. Source: Rahman and Skyllas-Kazacos [29]. Reproduced with permission of Elsevier. (b) Viscosity of different vanadium ion solutions as a function of temperature. Source: Xiao et al. [21]. Reproduced with permission of Royal Society of Chemistry.

that in sulfate solution over a wide temperature range, owing to the formation of dinuclear vanadium species like $V_2O_3^{4+}$ or $[V_2O_3Cl]^{3+}$ [38].

Li et al. [22] have further explored a mixed sulfate-chloride electrolyte to stabilize the vanadium species. In the mixed-acid electrolyte, concentrated vanadium solutions exhibited excellent thermal stability in a wide temperature range between −5 and 50 °C [22, 39]. The improved electrolytes stability was then studied by means of ^{35}Cl nuclear magnetic resonance (NMR) and ^{51}V NMR. It is considered that a soluble intermediate product of $VO_2Cl(H_2O)_2$ forms in the presence of the Cl^- ions in the catholyte [22], as shown in Eqs. (13)–(16):

$$\text{Catholyte}: VO^{2+} + H_2O \leftrightarrow VO_2^+ + 2H^+ + e^- \tag{13}$$

$$VO_2^+ + Cl^- \leftrightarrow VO_2Cl \tag{14}$$

$$\text{Anolyte}: V^{3+} + e^- \leftrightarrow V^{2+} \tag{15}$$

$$\text{Overall}: VO^{2+} + V^{3+} + Cl^- + H_2O \leftrightarrow VO_2Cl + V^{2+} + 2H^+ \tag{16}$$

This complexation with chloride and water slows down the formation of insoluble V_2O_5. A flow cell, using 2.5 M vanadium in mixed sulfate-chloride system (2.5 M SO_4^{2-} and 6 M Cl^-) [22], realized a 70% improvement in the volumetric energy density compared to that in the sulfate solution under ambient environment.

Subsequently, Vijayakumar et al. [40] further elucidated that the high thermal stability of VO_2^+ cations in the mixed-acid system can also be attributed to the formation of the chlorine bonded compound $[V_2O_3Cl_2(H_2O)_6]^{2+}$, which also inhibits the de-protonation and subsequent precipitation reactions.

Note that evaporation of hydrochloric acid and chlorine evolution side-reactions are inevitable at a high SOC or over long-term operation of the flow cell in the mixed-acid electrolyte [22], leading to corrosion issues. Concerning the thermal stability and safety issues, for the electrolyte with vanadium concentration between 1.6 and 2.4 M, the suggested concentration of hydrochloric acid and sulfuric acid is in the range of 6–6.4 M and 2–3 M, respectively [36, 41]. In addition, it was also found that in 2 M VO_2^+ + 2.5 M H_2SO_4 solution, the ionic conductivity increases from 410 to 480 mS cm^{-1} when the chloride ion concentration increases from 5.6 to 6.4 M [36].

Although a high H_2SO_4 concentration can help to improve the ionic conductivity and the thermal stability of VO_2^+, the diffusivities of vanadium ions decrease due to an increased viscosity. This causes a larger polarization in the electrode reactions, and accordingly a decrease in the voltage efficiency. Furthermore, the power loss, from electrolyte pumping, results in a reduction of the total energy efficiency of the system. In contrast to the increased viscosity with high H_2SO_4 concentrations, hydrochloric acid solutions of the same concentration can have about 30–40% lower viscosity. Therefore, it is expected that hydrochloride acid-based electrolytes could reduce the pumping energy consumption.

Other acids such as phosphoric acid and ethylenediaminetetraacetic acid (EDTA) were also tested [42], but they were not as effective as HCl. Mixed-acid solutions using methanesulfonic acid (MSA) (CH_3SO_3H) were found to be helpful for improving the solubility and stability, however, with a penalty of an increased ohmic resistance [43]. Moreover, the H_2SO_4—CH_3SO_3H mixture showed improved redox kinetics for the VO_2^+/VO^{2+} couple reaction and reduced mass transport resistance. A flow cell with 2 M VO^{2+} was able to deliver an initial energy density of 40 Wh l^{-1} at a high current density of 120 mA cm^{-2}, with a capacity loss of 20% after 30 charge/discharge cycles [43].

2.5 Additives for Vanadium Electrolytes

To improve the stability of concentrated vanadium solutions and to increase the energy density of vanadium RFBs, some additives have been employed.

Table 2 The influence of additives on the thermal stability of vanadium ions.

	Vanadium concentration (M)	Sulfate concentration (M)	*T* (°C)	Additives	Time for precipitation (d)	Reference
V^{2+}	2	5	−5	0.2 wt% PA	>90	[23]
	2	5	5		16 h	[42]
V^{3+}	2	5	−5		26	[23]
	2	5	−5	3 wt% Na_3PO_4	30	[23]
	2	5	−5	0.3 wt% PA	108	[23]
	2	6.5	5		4	[42]
	2	6.5	5	$(NH_4)_3PO_4$	40	[42]
VO^{2+}	2	5	−5		<18 h	[23]
	2	5	−5	3 wt% K_2SO_4	>11	[23]
	2	5	−5	3 wt% Na_3PO_4	>30	[23]
	2.3	5	−5	1.0 wt% PA	9	[23]
	4	3	4		<22	[44]
	4	3	4	3 wt% SHMP	>90	[44]
	4	3	4	2 wt% K_2SO_4	>90	[44]
VO_2^+	2	5	−5		>33	[23]
	2	5	−5	0.2 wt% PA	>90	[23]
	3	5	30	1 wt% H_3PO_4	47	[45]
	5	1.8	40	7 wt% CH_3SO_3H + 0.4 wt% PA	36	[23]

Skyllas-Kazacos et al. [44] introduced precipitation inhibitors to stabilize concentrated vanadium electrolytes at low temperatures. The influence of several different additives on the thermal stability of vanadium ion solutions is summarized in Table 2. While 4 M $VOSO_4$ solutions show precipitation after 22 days in 3 M H_2SO_4 at 4 °C, solutions containing 2 wt% K_2SO_4, 3 wt% sodium hexametaphosphate (SHMP), or 5 wt% urea show an induction time for precipitation of over 90 days [44]. It is believed that the additive species NH_4^+, PO_4^{3-}, HPO_4^{2-}, and $H_2PO_4^-$ decrease the rate of crystal growth of V_2O_5, by absorbing onto the surface of the nucleation sites. For instance, at 30 °C the induction time of a 3 M VO_2^+/5 M SO_4^{2-} electrolyte was extended to 47 days by addition of 1 wt% H_3PO_4, but just a few days at 50 °C [45, 46]. Although the thermal stability of VO_2^+ could be promoted with suitable inorganic additives, chemicals containing K^+ cations, phosphate and polyphosphate anions are not suitable because of the formation of $KVSO_6$ or $VOPO_4$ precipitates during flow cell operation [23]. Some inorganic additives could even allow vanadium ion concentrations up to 4 M using SHMP, K_2SO_4, and Li_2SO_4 species. Nevertheless, most of those additives suffer from long-term stability because of the occurrence of gas evolution or precipitation during the flow cell operation. So far, only a 3 M VO_2^+ electrolyte demonstrated stable capacity retention over 90 cycles at 30 °C with the employment of a 1 wt% H_3PO_4 + 2.5 wt% $(NH_4)_2SO_4$ [45].

Alternatively, organic additives, containing —COOH, —CO—, —OH, —SH or —NH_2 groups, can also suppress the crystal growth of V_2O_5 [44, 47]. Various stabilizing agents, including L-glutamic acid, MSA, aminomethyl sulfonic acid (AMSA), glucose, glycerol, thiols, poly(ethyleneimine)-based dendrimer and hexadecyl trimethyl ammonium bromide (CTAB), have been applied to enhance the thermal stability and electrochemical reversibility [23, 48, 49]. Meanwhile, some organic additives such as D-sorbitol, inositol, phytic acid, and trishydroxymethyl aminomethane can effectively promote the dispersion of $[VO_2(H_2O)_3]^+$ ions due to Columbic repulsion and steric hindrance. However, changes in solution color and presence of unwanted precipitates have been observed during the stability test [49]. Most of the low-molecular-weight organic additives, such as glycerol, fructose, oxalates, EDTA, and formic acid, with functional groups of C=C, OH, CHO, and C=O, are not stable in VO_2^+ solutions [23]. Recently, the large organic cation group of 1-butyl-3-methylimidazolium ($BMIm^+$) has been used to inhibit the aggregation of vanadium ions into V_2O_5 in the catholyte by Coulombic repulsion and steric hindrance [50]. ^{51}V NMR showed a change in the local coordination environment of vanadium species. In addition, improved thermal stability has been observed for the charged vanadium catholyte with $BMIm^+$ as additive.

Mousa and Skyllas-Kazacos [42] further investigated the effect of additives on the stability of 2 M V^{2+} and 2 M V^{3+} anolyte at low temperatures. In 2 M V^{2+}/5 M SO_4^{2-} solutions containing tungstic acid and sodium tungstate, no precipitation was observed over a long testing period. Nevertheless, formation of dark precipitates by oxidation of V^{2+} was observed. In flow cell tests, a 2 M vanadium electrolyte with 2 wt% $(NH_4)_3PO_4$ exhibited no precipitation over 250 cycles at a low temperature of 5 °C. Meanwhile, the low-molecular-weight organics, such as glucose, glycine, urea, maleic anhydride, and acrylic acid derivatives, only showed a negligible effect on the stability of concentrated V^{2+} solutions. In addition, polyacrylic acid (PAA) has been used as a suitable candidate for the anolyte at low temperatures. The 2 M V^{2+}/5 M SO_4^{2-} solution in the presence of 0.2 wt% PAA showed excellent stability over 90 days at −5 °C [23].

Note that the content of additives must be optimized because a large amount of additives will damage the hydrated layer of VO_2^+ ions, affecting the mass transport and increasing the ohmic polarization of the battery.

2.6 State-of-Charge (SOC)

Over charge/discharge cycling, vanadium ions, protons, sulfates and water transfer through the ion exchange membrane, and parasitic side-reactions may occur (as will be discussed in Section 3). This causes continuous changes in the volume, composition and concentration of the catholyte and the anolyte, and leads to a decrease in the cycling efficiencies and continuous capacity fading. Therefore, the battery management system requires sensors and control units to obtain real-time information about the oxidation states of vanadium ions, concentration of vanadium species, imbalance in the catholyte and anolyte, cell voltage, open circuit voltage (OCV) and pH value. After a certain number of cycles, rebalancing of the electrolytes is needed to return them to their

initial states. Accordingly, measurements and predictions of the SOC of the vanadium electrolytes are important for maintaining a long-term service life of the electrolytes, and for avoiding overcharging. The SOC is defined as below:

$$\text{Anolyte}: \text{SOC}_{\text{anolyte}} = [V^{2+}]/([V^{2+}] + [V^{3+}]) \tag{17}$$

$$\text{Catholyte}: \text{SOC}_{\text{catholyte}} = [VO_2{}^+]/([VO^{2+}] + [VO_2{}^+]) \tag{18}$$

As can be seen from Eqs. (17) and (18), a 100% SOC indicates a complete oxidation of $[VO^{2+}]$ to $[VO_2{}^+]$ in the catholyte, and a complete reduction of $[V^{3+}]$ to $[V^{2+}]$ in the anolyte. At this stage, the cell is fully charged. In contrast, at the fully discharged state, only $[VO^{2+}]$ and $[V^{3+}]$ exist in the catholyte and anolyte, respectively.

Typically, the SOC can be assessed by using a separate OCV cell [51]. The OCV cell is the same as the redox flow cell but without an electronic current. The OCV values reflect the potential difference of the two half-cells, and are associated with the concentrations of vanadium ions through the Nernst equation. Thus, from the measured OCV values, the ratio of vanadium species can be estimated. However, the cross-mixing of vanadium species and the transfer of water result in unknown concentrations in the Nernst equation. The electrode degradation also causes a drift of the OCV values over long-term operation. Thus, an accurate calculation is impossible.

In addition, due to the imbalance of electrolytes, the SOC for the anolyte and catholyte need to be determined individually. To tackle these issues, the open circuit potentials (OCP) of the two half-cells have been measured separately by using additional working and reference electrodes [52]. These electrodes, however, can be attacked or contaminated by the vanadium electrolytes. Alternatively, *in situ* measurements of the electrolyte conductivity have been performed to estimate the SOC [34]. The change in the electrolyte conductivity is mainly from the variation of the proton concentration during the flow cell cycling.

Changes of the vanadium valence states are associated with an alteration of the coordination environment of the different vanadium ions. These distortions in the coordination shapes together with the energy level change will trigger a shift in their absorption wavelength [53]. This allows to monitor the SOC also by *in situ* ultraviolet–visible (UV–VIS) spectroscopy, as has been recently studied by Hempelmann and co-workers [54, 55].

3 Membranes and Transport of Species

3.1 Function of the Membranes

Besides the redox electrolyte, membranes are one of the most critical components in vanadium flow batteries. They separate the anolyte and catholyte, and hinder the crossover of the redox-active species by having a low vanadium ion permeability. At the same time, they should show a high ionic conductivity for the charge-balancing ions (protons and/or sulfate ions) (Figure 5 [56]). In addition, they should have no electronic conductivity and help to seal the cells together

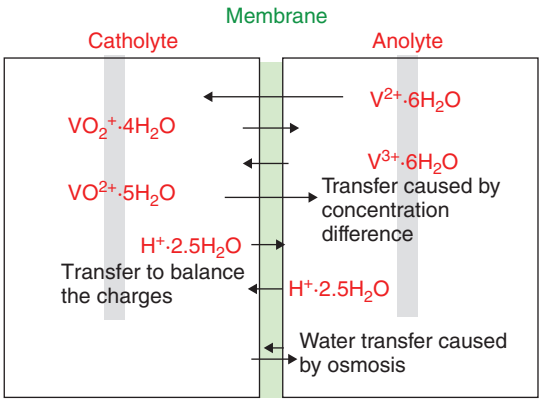

Figure 5 Illustration of the transport of ionic species and water through the membrane for the vanadium electrolytes. Source: Sun et al. [56]. Reproduced with permission of Elsevier.

with the gaskets. Further requirements are a high stability against the sulfuric acid in the anolyte and catholyte, and a high chemical stability against oxidative reagents (e.g. against VO_2^+).

A thin membrane would reduce material costs and ohmic resistance of the cell. However, diffusion of vanadium ions through the membrane increases with decreasing thickness. Consequently, a good compromise between vanadium crossover and membrane resistance must be studied experimentally. In order to achieve a long lifetime, perfluorinated polymer membranes with excellent chemical stability are preferred. However, synthesis of perfluorinated ion conducting polymers such as Nafion requires the handling of gaseous monomers, resulting in high fabrication costs [57]. Furthermore, fluorinated materials are less easy to recycle, e.g. burning wastes to regain all traces of vanadium would liberate highly corrosive hydrogen fluoride (HF).

3.2 Characterization Methods of Membranes

3.2.1 Swelling Behavior and Acid Absorption

The ionic groups in polymer electrolyte membranes strongly interact with water. In contact with vanadium anolyte and catholyte, membranes absorb significant amounts of sulfuric acid and water and swell (with changes in membrane thickness and area). This enlarges the hydrophilic domains and increases their connectivity, and consequently increases the conductivity and vanadium permeability. For practical reasons, it is important to know the swelling properties of the membranes in order to reduce membrane losses during cell assembly and to estimate the right thickness. While the measurements of the swelling behavior are simple, care needs to be taken that measurements should be performed within a short duration since water-swollen membranes lose about half of their water contents within about only two minutes. In addition, it needs to be considered that membranes are sometimes cast from aprotic polar solvents like dimethylacetamide (DMAc), which have a high boiling point and are difficult to be fully removed.

Their residues can easily constitute up to 50% of the membrane weight. Therefore, the weight and dimensions of wet membrane should be measured first, and the dry membrane subsequently, assuming that all solvents leach out into the solution in this step:

$$S_{x,y,z}\,(\%) = \frac{(D_{\text{wet}} - D_{\text{dry}})}{D_{\text{dry}}} \tag{19}$$

$$\text{weight gain}\,(\%) = \frac{(m_{\text{wet}} - m_{\text{dry}})}{m_{\text{dry}}} \tag{20}$$

where S is the swelling ratio, and D and m are the dimensions and mass of the membrane in the indexed states of "wet" or "dry."

3.2.2 Permeability and Crossover

Diffusion of vanadium ions through membranes can be easily measured and is commonly used to evaluate the suitability of the membranes. These tests ignore that crossover in the operating system not only depends on concentration-driven diffusion, but also on migration in the electric field, as described by the Nernst–Planck equation (Eq. (21)), in which the first term describes the flux of ions through a membrane by diffusion (Fick's law), and the second one by migration:

$$J = -D\nabla c - z\mu Fc\nabla\varphi \tag{21}$$

J is the flux of ions, D is the diffusion coefficient, c is the concentration of species in the membrane, z is the charge of the ion, μ is the ion mobility, F is the Faraday constant, and φ is the potential [58].

As a consequence, thinner membranes usually show a lower Coulombic efficiency in operating vanadium RFBs than thicker ones, due to a high diffusion level. In some cases, however, the opposite may be observed, e.g. when a membrane shows both very low permeability and low conductivity. In this case, by decreasing the thickness, crossover of vanadium species increases only slightly. Due to a high membrane resistance, however, the reduced thickness has a noticeable effect on the average charging voltage, resulting in less migration. The overall effect is an increased Coulombic efficiency, even though the membrane thickness decreases [59].

Diffusion-driven vanadium ion permeability of the membranes can be measured through separating a vanadium-rich solution ("A") and a vanadium-lean solution ("B") by a membrane. Slowly, vanadium ions cross over into the receiving solution by diffusion, and a quasi-linear increase of the concentration can be observed, which can be mathematically described by the equation, Eq. (22):

$$C_{\text{B}}(t) = \frac{A}{V_{\text{B}}}\frac{P}{L}\,C_{\text{A}}(t - t_0) \tag{22}$$

in which C_{A} and C_{B} are the concentration of solution "A" and "B," A is the active area of the membrane, V_{B} is the volume of the vanadium-lean solution, L is the thickness of the membrane, t is the time, and P is the permeability coefficient.

The latter can be obtained by transformation into:

$$P = \frac{1}{C_A}\left(\frac{\Delta C_{B(t)}}{\Delta t}\right)\left(\frac{LV_B}{A}\right) \tag{23}$$

Here, the second term in Eq. (23) is the slope of the quasi-linear trend line, when the concentration of permeated vanadium is plotted against time. Since P is normalized by the membrane thickness, the permeability coefficient is a material property and should be the same for membranes of different thickness. Dividing P by the membrane thickness gives the permeation flux of ions per time and membrane area. This allows to compare two distinct membranes.

For the studied Nafion 212 membranes, reported values for $P(VO_2^+)$ are in the range of 10^{-12}–10^{-11} m^2 s^{-1} [60–62]. Differences originate from the use of different acid electrolytes (higher acid and vanadium concentrations are expected to reduce the water absorption and thus swelling), different thickness values (e.g. thickness of the membrane was measured before or after the test) and different hygro-thermal histories of the membrane processing (e.g. how long was it equilibrated, and in which solutions). Another important parameter is the temperature. Most groups report the diffusion values at "room temperature," and do not control this further. Also the geometry of the glass ware and stirring speed of the solutions play a role. If the solutions are not effectively stirred, the concentration of the solutions close to the membrane will differ from that of the bulk solutions, reducing the concentration gradient over the membrane. Finally, there could be a difference in how the vanadium ion concentration was determined. Typically, UV–VIS spectra are used for such purpose. Depending on the concentration of the vanadium ion containing solutions, different peaks or peak positions may be chosen for the analysis. An overview can be found in the literature [63, 64]. For example, V^{2+} has peaks at 283, 373, 567, and 800 nm. The peak at 283 nm is the most intensive peak and even dilution of the sample solution may be required. But only the peak at 800 nm has no overlapping with the signals of V^{3+}.

While all vanadium species have a different permeability, most work focuses on VO_2^+, because the composition of ions depends on the SOC and therefore is not well defined, and $VOSO_4$ is commercially available and has a lower risk to be oxidized or reduced than V^{2+} or VO_2^+.

3.2.3 Conductivity and Resistance

Conductivity is used to describe a membrane material, while area specific resistance (ASR) describes a membrane of a certain thickness. For the vanadium RFB application, the ASR with a unit of $\Omega\,cm^2$ of the membranes is the parameter which defines their performance. It is linked to the through-plane conductivity (σ) of the membranes by:

$$\sigma(S\ cm^{-1}) = \frac{\text{membrane thickness}}{\text{ASR}} \tag{24}$$

Therefore, a poor conductivity can be compensated in the vanadium RFB by preparing a thinner membrane, if the mechanical properties and vanadium permeability of the polymers allow it.

For the conductivity measurement, a membrane sample is immersed in the electrolyte solution and two electrodes (e.g. gold coated metal discs) are arranged on both sides of the membrane in a known distance [65]. If the membrane resistance is high enough, a single measurement may give a correct value. However, in most cases it is necessary to repeat the measurement with membrane samples of different thickness. Assuming that the interfacial resistance between two membrane samples is negligible, different thicknesses can also be obtained by stacking membrane samples. A plot of the resistance (measured typically by electrochemical impedance spectroscopy (EIS)) versus the membrane thickness or thickness of different membrane stacks then gives a linear trend. The *y*-axis intercept is the sum of the ionic resistance of the electrolyte, the electronic resistance of the cables and the interfacial resistances of electrode/electrolyte and electrolyte/membrane. The conductivity is then calculated from the slope of the curve by:

$$\sigma(\mathrm{S\,cm^{-1}}) = \frac{1}{(\mathrm{slope} \cdot \mathrm{membrane\ area})} \tag{25}$$

Usually, researchers do not report the conductivity in vanadium containing electrolytes, but that in sulfuric acid, because the composition of the vanadium ions in the electrolytes changes during charging and discharging, and is therefore not well defined. This leads to an overestimation of the conductivity: (i) The increased concentration of ions in the electrolyte is expected to reduce the water uptake of the membrane by increasing the osmotic pressure. (ii) In cation exchange membranes, some of the protons will be exchanged for vanadium ions; the extent to which this will happen depends on the membranes' selectivity and the concentrations of metal ion and acid. For example, it was shown that Nafion 112 membranes equilibrated in metal ion containing solutions showed a conductivity of ca. 95 mS cm^{-1} at 80 °C, 100% relative humidity up to an iron concentration of ca. 0.2 ng ml^{-1}. Above that concentration, the conductivity started to decrease down to about 40 mS cm^{-1} at 0.5 ng_{iron} ml^{-1} [66]. This indicates that metal ion impurities need to be absolutely prevented (e.g. no metal tweezers should be used for handling membranes after equilibration in acidic solutions). Changing the electrolyte solution from 2.6 M sulfuric acid to 2.6 M sulfuric acid containing 1.5 M $VOSO_4$ reduced the conductivity of Nafion 212 from 45 to 23 mS cm^{-1}, and that of a sulfonated para-polybenzimidazole (PBI) membrane from 593 to 242 mS cm^{-1} [67].

3.2.4 Chemical Stability of Membranes

Most membrane materials, which are considered for use in vanadium RFBs, are known to be stable against water and acids. Thus, chemical stability is mainly discussed for stability against VO_2^+ ions. These tests are straightforward, membrane samples are immersed in solutions containing VO_2^+ ions in sulfuric acid, e.g. fully charged electrolyte, for a time of several days or weeks. Degradation is then monitored from the appearance of the membrane (e.g. sulfonated polysulfones will disintegrate into pieces in this test [68]), the weight loss of the membrane, and by using UV–VIS spectroscopy for the formation of VO^{2+} (which is formed when VO_2^+ reacts with the membrane)

[65]. For poly(arylene ether) membranes, the attack of VO_2^+ is believed to occur at the ether bonds [69]. The following chain scission leads to reduced molecular weight of the polymer, and therefore loss of mechanical strength and disintegration. A blind test of the VO_2^+ solution without membrane sample gives access to the initial VO^{2+} concentration and formation of VO^{2+} by reaction with impurities, which may be present in the solution or the vial and lid.

3.3 Membrane Types

Membranes for vanadium RFB can be categorized into five general groups [15]: perfluorinated and non–fluorinated cation exchange membranes, anion exchange membranes (AEM), nanofiltration membranes, and acid doped PBI membranes (Table 3).

Perfluorinated membranes (e.g. Nafion) are the most commonly employed membranes. They are most stable against the oxidative VO_2^+ ions, and have a high proton conductivity. However, they also show a high vanadium permeability and therefore a poor proton/vanadium selectivity. Accordingly, thick Nafion membranes, such as Nafion 115 with a thickness of 125 µm, are often used to alleviate the cross-mixing [70–72]. Nevertheless, the thick membrane leads to an increase in the ASR, which is relevant to the voltage efficiency. By changing the density of ionic groups (e.g. reducing the ion exchange capacity) of Nafion membranes, vanadium ion permeability can be decreased, but only together with the conductivity. Unfortunately, such modified membranes are not commercially available yet and cannot be easily synthesized [73].

In order to reduce the costs, to alleviate the use of fluorinated materials, and to reduce the vanadium crossover, hydrocarbon based cation exchange membranes have been developed. In these membranes, the phase separation between sulfonated groups and polymer backbone is less pronounced. In

Table 3 Membrane types and their general properties.

Type	Example	Conductivity	Vanadium ion permeability	Chemical stability
Perfluorinated cation exchange membranes	Nafion	High	High	High
Hydrocarbon based cation exchange membranes	Sulfonated polysulfone	High	Average	Poor
AEM	Polysulfone with quaternary ammonium groups	Average	Low	Poor
Nanofiltration membranes	PIM1, polysulfone, etc.	Average-high	Average-high	Average (expected)
Acid doped membranes	PBI	Low	Low	High
	Sulfonated, pre-swollen PBI	High	High	High

addition, the aromatic sulfonic acid groups are less acidic than the sulfonic acids groups in Nafion, which have a lower pK_a value due to the electron-withdrawing effect of the fluorinated side chains [74]. This leads to narrower, less connected hydrophilic domains and thus a more tortuous pathway for the diffusion of vanadium ions. This further results in an increase in the Coulombic efficiency in comparison to Nafion-based vanadium RFBs. The major drawback for hydrocarbon based cation exchange membranes is their susceptibility to degradation by the oxidative VO_2^+ ions [61, 75].

By definition, AEM should not transfer metal cations. But since the Donnan exclusion of cations for the membranes is most effective in diluted solutions [76], transfer of metal ions through an AEM cannot be completely avoided. At the high concentrations used in vanadium RFB electrolytes, it is expected that a significant amount of co-ions is dissolved in the membrane. Therefore, also AEM possess a measurable vanadium permeability, which, however, is lower than that of cation exchange membranes [61, 77]. Since hydroxide ions have a 1.8 times lower molar conductivity than protons [78], AEM often have a higher ASR than Nafion membranes. Similar to hydrocarbon-based cation exchange membranes, AEM are easily attacked by VO_2^+, unless the polymer backbone is fluorinated and free of ether bonds [69].

Nanofiltration membranes have so small pores that particles or molecules with a hydrodynamic radius larger than 2 nm cannot pass [79]. While a pore size of 2 nm would not be sufficient to separate between charge-balancing ions (<3.01 Å) and hydrated multivalent vanadium ions (>3.78 Å), nanofiltration membranes with very narrow pore dimensions should be able to block the transfer of vanadium ions by size-exclusion effect. Cation exchange membranes with pore sizes in the range of 3.98–7.56 Å and AEM with pores sizes of 6.02–7.56 Å are suggested to selectively transport charge-balancing ions [80]. For comparison, the dimensions of the hydrophilic domains in Nafion are in the range of 4 nm, and connections between the domains have a dimension of about 1 nm [81]. This indicates that cation exchange membranes or AEM need to have very low ion exchange capacities (low density of ionic groups) to prevent absorption of water and swelling of the hydrophilic domains. In fact, ionic groups do not seem to be necessary, and a high selectivity of protons over VO^{2+} was achieved by using PIM-1, a polymer of intrinsic microporosity as selective layer on a porous polyacrylonitrile membrane [82]. Also poly(ether sulfone) [83] and polyacrylonitrile-based asymmetric porous membranes with a thin selective layer [84] were found to have a high selectivity. An anticipated problem could be the expected reactivity of these polymers against VO^{2+}, which could limit their lifetime.

PBI membranes are the latest addition to the group of membranes used in vanadium RFB [85], and show a high potential to substitute the bench-mark Nafion membranes. A vanadium RFB using a porous O-PBI membrane showed a stable cycling behavior of over 13 500 cycles at a current density of 80 mA cm^{-2} [86]. PBI is a high-performance polymer with two amine and two imine nitrogen groups per repeat unit (Figure 6). Pristine PBI is practically insulating for conducting ions, but in contact with sulfuric acid (e.g. the vanadium RFB electrolyte), the nitrogen functionalities are protonated. This introduces two positive charges

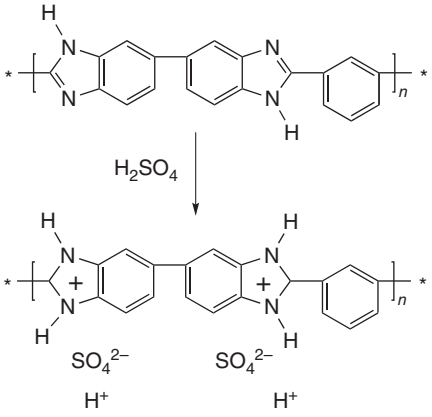

Figure 6 Chemical structure of PBI and its structure after doping with sulfuric acid.

per repeat unit and about 2 mol of free, mobile HSO_4^- [59]. This increases the conductivity to about 5 mS cm^{-1}, which is low in comparison to that of Nafion (40–80 mS cm^{-1}). However, the high ASR of PBI membranes can be partially compensated by using thin membranes. A thin PBI membrane with a thickness of 15 µm can be operated well in a vanadium RFB [59]. Moreover, a 4 µm PBI blocking layer on porous supports showed a good performance [87]. The use of very thin PBI layers is enabled by the high tensile strength (67 MPa), Young's modulus (1.4 GPa) and high elongation at break (39%) of sulfuric acid doped PBI [65], and the very low vanadium permeability. The combination of a high positive charge density on the polymer chain and a dense morphology (e.g. no phase separation into large, well connected hydrophilic domains) effectively hinders diffusion of vanadium species. In one *ex-situ* test, diffusion of VO^{2+} was so slow that it could not be observed even after 10 days [88].

Because of the positively charged polymer backbone, PBI membranes effectively repel vanadium cations. Aromatic ether groups can be easily avoided. In a simple explanation, when oxidizing VO_2^+ degrades a polymer, electrons are transferred from the polymer to VO_2^+. This seems to be more difficult when the backbone has a low electron density (as in protonated PBI).

Commercial PBI membranes cast from organic solvents have a rather low uptake of sulfuric acid and narrow channel structures. Pre-swelling in phosphoric acid increases the conductivity [89]. An extreme case is sulfonated *para*-PBI membranes cast from a polyphosphoric acid solution. These membranes have such an open structure that the conductivity of sulfuric acid doped membranes was reported to reach above 500 mS cm^{-1}. A drawback is the increased permeability. However, at a high current density of 500 mA cm^{-2}, a Coulombic efficiency over 95% and an energy efficiency over 70% was obtained [67]. In conclusion, by rationally selecting the polymer chemistry [62, 67, 90] and membrane fabrication process [67, 89], key performance parameters of conductivity, ASR and permeability of the PBI-based membranes can be freely adjusted to a large extent.

Several engineering strategies are feasible to develop better-performing vanadium RFB membranes, including (i) mechanical reinforcement by porous supports, which potentially also lowers the overall material costs [91], (ii) preparation of polymer blends [65, 92], and (iii) nanocomposite membranes [93, 94] to increase stability and to decrease vanadium permeability. Furthermore, layered membranes, consisting of a highly conductive/permeable layer and a vanadium blocking layer of lower conductivity like PBI [58, 87, 88, 95], are interesting to be applied in the near future.

4 Electrode Materials

Metal-based electrodes, such as lead, platinum, gold, titanium, and metal oxide coated dimensionally stable electrodes (dimensionally stable anodes, which are widely used in chlor-alkali electrolysis [96]), have been previously investigated for vanadium RFBs [12]. Although they exhibited electroactivity for the redox reactions of vanadium species, their widespread applications are restricted by either a high cost, or passivation. Alternatively, various carbon electrode materials, such as carbon felt, graphite felt, carbon cloth and carbon paper (as shown in Figure 7), with low cost, but high electrical conductivity, porosity, good acid resistance and acceptable electrochemical stability have been practically used for vanadium RFBs [97, 98]. The electrode surface provides the reactions sites, and the pores and the three-dimensional network structures allow the circulation of the vanadium redox fluids. Meanwhile, the pressure drop and the pumping power are associated with the electrode porosity and the compression ratio upon assembling them into the cell.

4.1 Electrode Reactions

During charge/discharge, the efficiency loss arising from the activation polarization mainly originates from the kinetics of the electrode reactions (Eqs. (1) and (2)). Therefore, the types of electrode materials [99] and their precursors [100], morphologies, porosities play a key role for improving the voltage efficiency of the vanadium RFBs (Figure 7). Sun and Skyllas-Kazacos [101, 102] and Qiu and

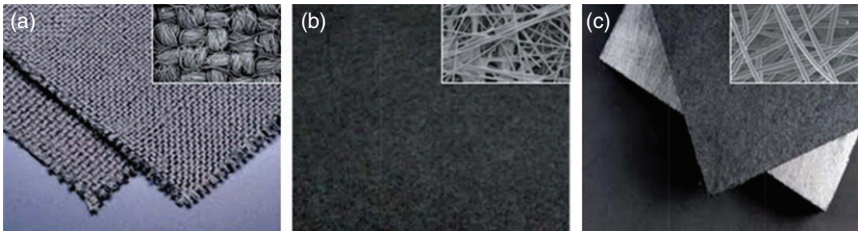

Figure 7 Carbon-based electrodes for vanadium RFBs. (a) carbon cloth, (b) carbon paper, and (c) carbon felt. Source: Kim et al. [97]. Reproduced with permission of Royal Society of Chemistry.

co-workers [103] proposed that the surface oxygen functional groups (C—OH as shown in Figures 8a,b, C—OOH as shown in Figure 8c) on the surface of carbon electrodes function as active sites for the redox reactions of vanadium species. For charging, these reactions proceed through bulk diffusion of reactants, ion exchange (VO^{2+} with H^+ of the phenolic groups in catholyte, V^{3+} with H^+ in anolyte), oxygen atom transfer (from C—O of the functional groups to VO^{2+}, forming VO_2^+), electron transfer, and back diffusion of products. During the discharge, the reverse processes occur. Two-dimensional graphene oxide electrodes (Figure 8d) that can provide high surface area have been applied with similar reaction mechanism [97, 105].

With the involvement of oxygen atom transfer in electrode reactions, the electrode surface is therefore generally processed by chemical methods, such as acidic and thermal treatment of carbon materials [101, 102, 106], to increase the content of the oxygen functional groups. Through the surface treatment, chemical doping [107, 108] and the application of catalysts on the surface of carbon electrodes (Figure 8e) [104], the power performance has been largely improved [109, 110]. Such performance enhancement allows significant decrease in the stack costs per kilowatt.

4.2 Carbon Paper Electrodes and "Zero-Gap" Concept of Cell Configuration

By reducing the electrode thickness from the ~mm scale of graphite felt electrodes down to ~micrometer scale, thin carbon paper electrodes have been applied in a "zero-gap" cell architecture for vanadium RFBs [111], which exhibited an improved limiting current density and a high peak power density. Accordingly, specific flow field and channel configurations have been designed to enhance the contact between the electrolyte and electrode, and the penetration of vanadium electrolytes into the porous electrode [112]. The electrodes and membrane can form a membrane-electrode assembly (MEA) structure, which is structurally similar to that used in proton exchange membrane (PEM) fuel cells. Such thin carbon paper electrodes enabled by flow field design result in a smaller ohmic loss, compared to that of the thick felt electrodes [11].

Flow channels should be designed to maximize the utilization of vanadium electrolytes and the reaction turnover rates, and meanwhile to minimize the pressure drops and pump losses. Optimization of cell and stack performance should also consider the properties of the employed vanadium electrolytes such as concentration and viscosity. The serpentine flow field (SFF) (left column in Figure 9) allows a fast flow of electrolytes and a low pressure drop, but only a small fraction of the vanadium electrolytes penetrates into the carbon electrodes [11]. For the interdigitated flow field (IFF), all electrolytes are forced to flow through the porous electrodes, leading to however a large pressure drop and energy consumption for the pumping. Furthermore, the flow behavior depends on the channel width and depth, and the landing width. Further new flow field designs have been reviewed elsewhere [11].

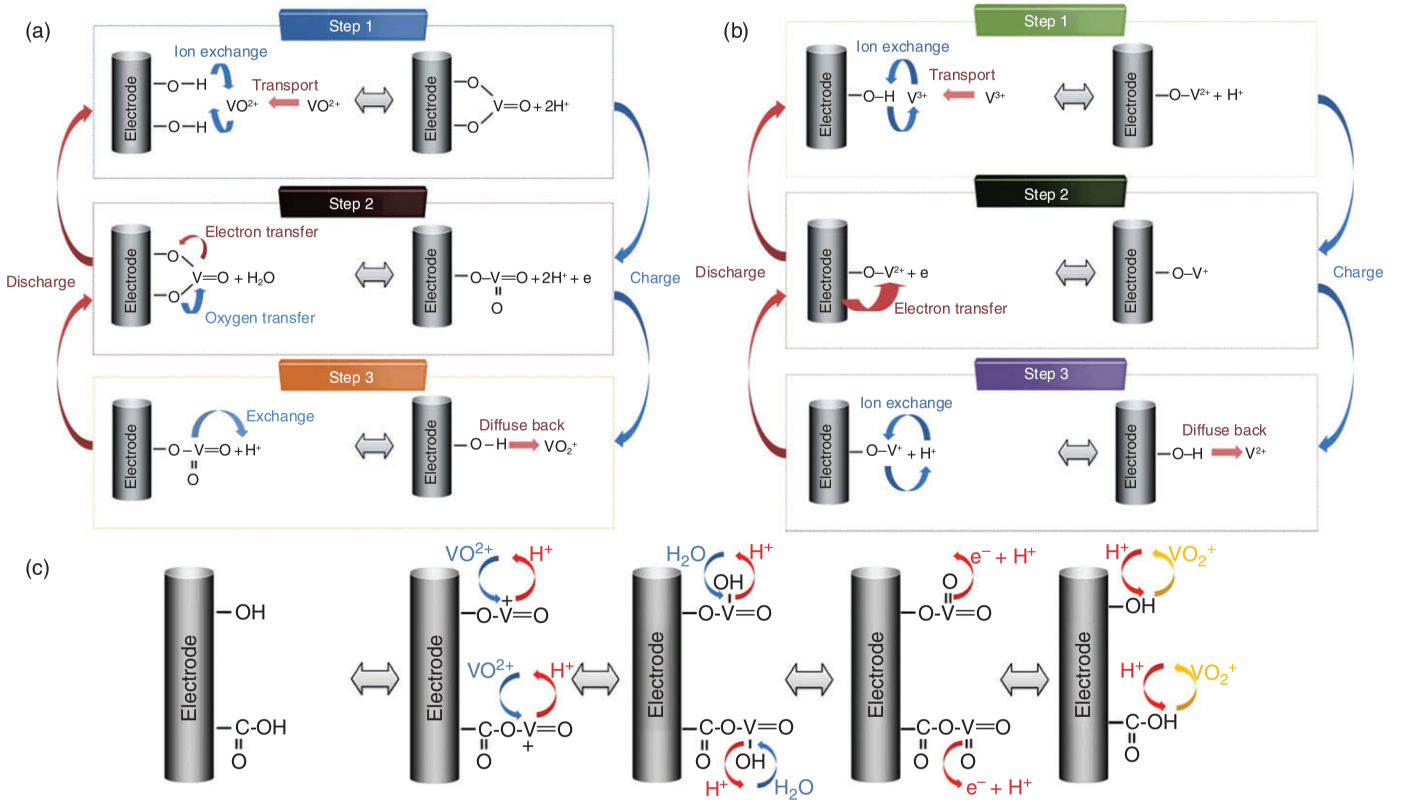

Figure 8 Proposed redox reaction mechanisms of vanadium species on the surface of carbon electrodes with (a), (b) C—OH functional groups, and (c) C—OOH functional groups. Source: Kim et al. [97]. Reproduced with permission of Royal Society of Chemistry. (d) Two-dimensional graphene oxide electrode. Source: Kim et al. [97]. Reproduced with permission of Royal Society of Chemistry. (e) Carbon electrodes with catalyst particles. Source: Zhou et al. [104]. Reproduced with permission of Royal Society of Chemistry.

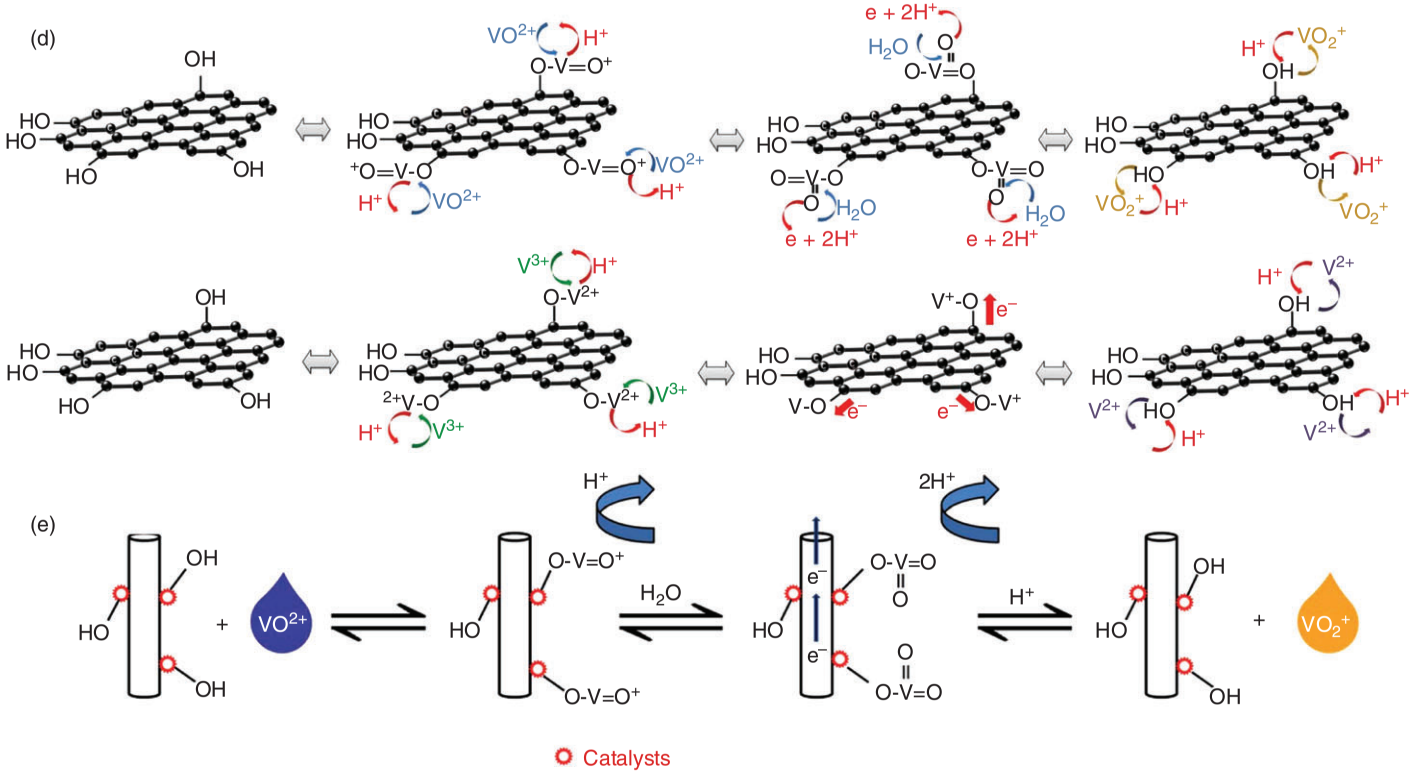

Figure 8 (*Continued.*)

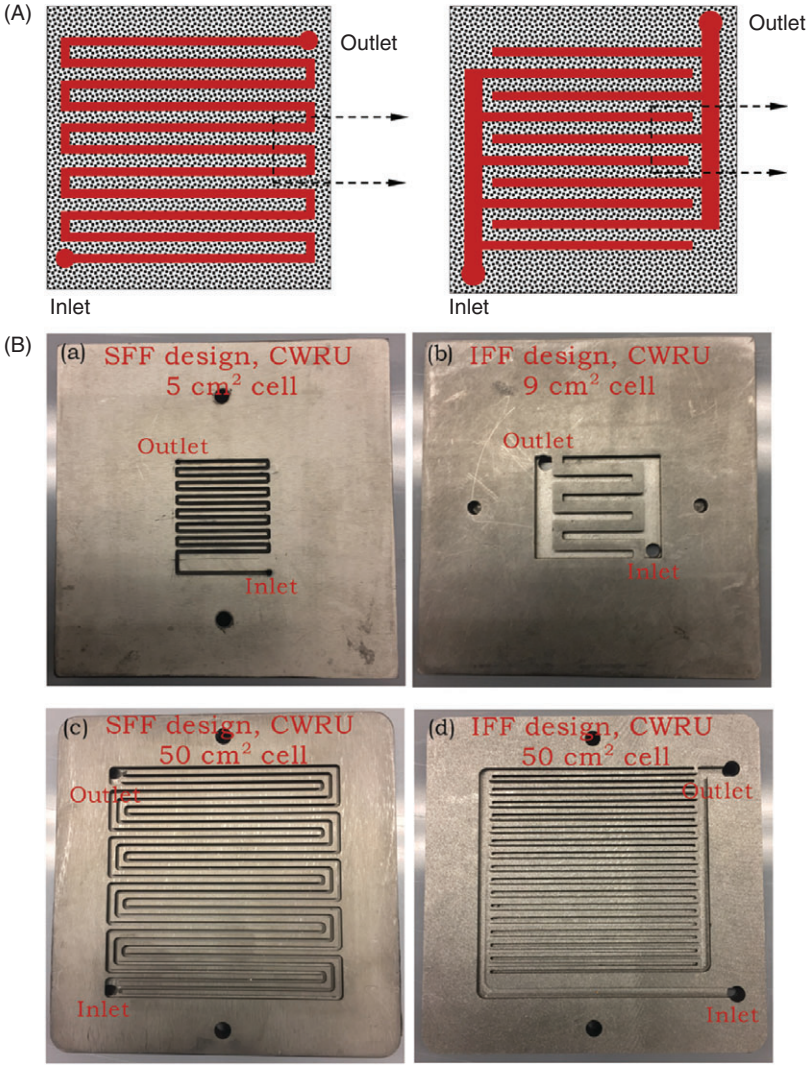

Figure 9 (A) Comparison of two different flow fields: serpentine flow field (SFF, on the left) and interdigitated flow field (IFF, on the right). (B) Pictures of flow field designs with different channel width and depth, landing width. Source: Ke et al. [11]. Reproduced with permission of Royal Society of Chemistry.

It is difficult to optimize the performance exclusively by experimental methods [113]. Simulation approaches have been developed to estimate the flow distribution, pressure distribution and local current density, in order to improve the overall operating efficiencies of the system and the power output [114–118].

4.3 Degradation Study of Carbon Electrodes

The performance loss arising from carbon electrode degradation in vanadium RFBs has been recently studied by electrochemical and spectroscopic techniques

[119]. The loss of electroactive surface area of carbon electrodes after prolonged electrochemical cycling has been recognized from EIS with a decrease in the double layer capacitance, and from cyclic voltammetry measurements with a decrease in the peak current [120, 121]. Moreover, it was found that electrode degradation is related to the applied cutoff voltages for the charge/discharge cycling of vanadium RFBs [122]. With the involvement of hydrogen evolution at the negative half-cell, or the CO_2 evolution at the positive half-cell at the high cutoff voltage of 1.8 V, a high rate of degradation of the electrode was observed [122]. This occurs together with an imbalance of the vanadium electrolytes. These experiments were performed for the diagnostics and optimization of vanadium RFB systems in order to maximize the system's output without causing significant parasitic reactions and degradation.

5 Conclusions

Green and sustainable energy sources will successively replace traditional energy resources. Vanadium RFBs, as promising stationary energy storage systems that can be integrated with the wind and solar power, have been extensively studied, including the detailed evaluation of the electrolyte properties (such as the synthesis methods of vanadium electrolytes, the possible maximum concentration of vanadium ions, influence of the supporting acidic electrolytes, thermal and chemical stability, application of additives and methods for the determination of the SOC), selection and tests of different types of membranes (ion selective membranes, and porous, size-exclusion membranes), design and optimization of the electrode materials (such as the improvement of the reaction kinetics by surface processing, and by using catalysts). The overall performance for the flow battery operation is governed by these parameters. Future work to reduce the costs for the vanadium extraction, membrane, cell components and their processing is needed. Except for the laboratory-scale single cell tests, commercial applications need rational design of the stacks to maximize the energy efficiency and the power output as well.

Utility-scale energy storage applications require safer, more scalable, longer-lasting batteries. For this, vanadium RFBs, using nonflammable aqueous systems, with decoupled energy storage and power generation and an expected service-life up to ~decades, may outperform the traditional Li-ion batteries. Furthermore, lithium is more expensive than vanadium, and Li-ion batteries have a relatively short service life of ~years. Fast and widespread market penetration of vanadium RFBs is thus expected in the foreseeable future.

References

1 Sum, E., Rychcik, M., and Skyllas-Kazacos, M. (1985). Investigation of the V(V)/V(IV) system for use in the positive half-cell of a redox battery. *J. Power Sources* 16: 85–95.

2 Sum, E. and Skyllas-Kazacos, M. (1985). A study of the V(II)/V(III) redox couple for redox flow cell applications. *J. Power Sources* 15: 179–190.

3 Green, M.A., Rychcik, M., Robins, R.G. et al. (1986). New all-vanadium redox flow cell. *J. Electrochem. Soc.* 133: 1057–1058.

4 Kazacos, M. and Skyllas-Kazacos, M. (1989). Performance characteristics of carbon plastic electrodes in the all-vanadium redox cell. *J. Electrochem. Soc.* 136: 2759–2760.

5 Rychcik, M. and Skyllas-Kazacos, M. (1987). Evaluation of electrode materials for vanadium redox cell. *J. Power Sources* 19: 45–54.

6 Holland-Cunz, M.V., Cording, F., Friedl, J. et al. (2018). Redox flow batteries – concepts and chemistries for cost-effective energy storage. *Front. Energy* 12: 198–224.

7 Chen, R. (2019). Toward high-voltage, energy-dense, and durable aqueous organic redox flow batteries: role of the supporting electrolytes. *ChemElectroChem* 6: 603–612.

8 Noack, J., Roznyatovskaya, N., Herr, T. et al. (2015). The chemistry of redox-flow batteries. *Angew. Chem. Int. Ed.* 54: 9776–9809.

9 Pan, F. and Wang, Q. (2015). Redox species of redox flow batteries: a review. *Molecules* 20: 20499–20517.

10 Ventosa, E., Buchholz, D., Klink, S. et al. (2015). Non-aqueous semi-solid flow battery based on Na-ion chemistry. P2-type $Na_xNi_{0.22}Co_{0.11}Mn_{0.66}O_2$–$NaTi_2(PO_4)_3$. *Chem. Commun.* 51: 7298–7301.

11 Ke, X., Prahl, J.M., Alexander, J.I.D. et al. (2018). Rechargeable redox flow batteries: flow fields, stacks and design considerations. *Chem. Soc. Rev.* 47: 8721–8743.

12 Ding, C., Zhang, H., Li, X. et al. (2013). Vanadium flow battery for energy storage: prospects and challenges. *J. Phys. Chem. Lett.* 4: 1281–1294.

13 Minke, C. and Turek, T. (2018). Materials, system designs and modelling approaches in techno-economic assessment of all-vanadium redox flow batteries – a review. *J. Power Sources* 376: 66–81.

14 Gubler, L. (2019). Membranes and separators for redox flow batteries. *Curr. Opin. Electrochem.* 18: 31–36.

15 Ye, R., Henkensmeier, D., Yoon, S.J. et al. (2018). Redox flow batteries for energy storage: a technology review. *J. Electrochem. Energy Convers. Storage* 15: 010801.

16 Yuan, Z., Zhang, H., and Li, X. (2018). Ion conducting membranes for aqueous flow battery systems. *Chem. Commun.* 54: 7570–7588.

17 Heo, J., Han, J.-Y., Kim, S. et al. (2019). Catalytic production of impurity-free $V^{3.5+}$ electrolyte for vanadium redox flow batteries. *Nat. Commun.* 10: 4412.

18 Lu, W., Li, X., and Zhang, H. (2018). The next generation vanadium flow batteries with high power density – a perspective. *Phys. Chem. Chem. Phys.* 20: 23–35.

19 Choi, C., Kim, S., Kim, R. et al. (2017). A review of vanadium electrolytes for vanadium redox flow batteries. *Renew. Sustain. Energy Rev.* 69: 263–274.

20 Lourenssen, K., Williams, J., Ahmadpour, F. et al. (2019). Vanadium redox flow batteries: a comprehensive review. *J. Energy Storage* 25: 100844.

21 Xiao, S., Yu, L., Wu, L. et al. (2016). Thermal stability of concentrated V(V) electrolytes in the vanadium redox cell. *Electrochim. Acta* 187: 525–534.

22 Li, L., Kim, S., Wang, W. et al. (2011). Effects of additives on the stability of electrolytes for all-vanadium redox flow batteries. *Adv. Energy Mater.* 1: 394–400.

23 Zhang, J., Li, L., Nie, Z. et al. (2011). Broad temperature adaptability of vanadium redox flow battery–part 1: electrolyte research. *J. Appl. Electrochem.* 41: 1215–1221.

24 Skyllas-Kazacos, M., Menictas, C., and Kazacos, M. (1996). A stable vanadium redox-flow battery with high energy density for large-scale energy storage. *J. Electrochem. Soc.* 143: L86–L88.

25 Kausar, N., Howe, R., and Skyllas-Kazacos, M. (2001). Raman spectroscopy studies of concentrated vanadium redox battery positive electrolytes. *J. Appl. Electrochem.* 31: 1327–1332.

26 Vijayakumar, M., Li, L., Graff, G. et al. (2011). Towards understanding the poor thermal stability of V^{5+} electrolyte solution in vanadium redox flow batteries. *J. Power Sources* 196: 3669–3672.

27 Kim, S., Choi, C., Kim, R. et al. (2016). Temperature-dependent ^{51}V nuclear magnetic resonance spectroscopy for the positive electrolyte of vanadium redox flow batteries. *RSC Adv.* 6: 96847–96852.

28 Cao, L., Skyllas-Kazacos, M., Menictas, C. et al. (2018). A review of electrolyte additives and impurities in vanadium redox flow batteries. *J. Energy Chem.* 27: 1269–1291.

29 Rahman, F. and Skyllas-Kazacos, M. (2009). Vanadium redox battery: positive half-cell electrolyte studies. *J. Power Sources* 189: 1212–1219.

30 Rahman, F. and Skyllas-Kazacos, M. (1998). Solubility of vanadyl sulfate in concentrated sulfuric acid solutions. *J. Power Sources* 72: 105–110.

31 Zhao, J.-X., Wu, Z.-H., Xi, J.-Y. et al. (2012). Complexes derived from strong field ligands. XIX. magnetic properties of transition metal derivatives of 4,4′,4″,4‴-tetrasulfophthalocyanine. *J. Inorg. Mater.* 27: 469–474.

32 Zhao, Y., Liu, L., Qiu, X. et al. (2019). Revealing sulfuric acid concentration impact on comprehensive performance of vanadium electrolytes and flow batteries. *Electrochim. Acta* 303: 21–31.

33 Corcuera, S. and Skyllas-Kazacos, M. (2012). State-of-charge monitoring and electrolyte rebalancing methods for the vanadium redox flow battery. *Eur. Chem. Bull.* 1: 511–519.

34 Skyllas-Kazacos, M. and Kazacos, M. (2011). State of charge monitoring methods for vanadium redox flow battery control. *J. Power Sources* 196: 8822–8827.

35 Jing, M., Wei, Z., Su, W. et al. (2016). Improved electrochemical performance for vanadium flow battery by optimizing the concentration of the electrolyte. *J. Power Sources* 324: 215–223.

36 Yang, Y., Zhang, Y., Tang, L. et al. (2019). Investigations on physicochemical properties and electrochemical performance of sulfate-chloride mixed acid electrolyte for vanadium redox flow battery. *J. Power Sources* 434: 226719.

37 Skyllas-Kazacos, M. (2003). Novel vanadium chloride/polyhalide redox flow battery. *J. Power Sources* 124: 299–302.

38 Kim, S., Vijayakumar, M., Wang, W. et al. (2011). Chloride supporting electrolytes for all-vanadium redox flow batteries. *Phys. Chem. Chem. Phys.* 13: 18186–18193.

39 Wang, W., Nie, Z., Chen, B. et al. (2012). A new Fe/V redox flow battery using a sulfuric/chloric mixed-acid supporting electrolyte. *Adv. Energy Mater.* 2: 487–493.

40 Vijayakumar, M., Wang, W., Nie, Z. et al. (2013). Elucidating the higher stability of vanadium(V) cations in mixed acid based redox flow battery electrolytes. *J. Power Sources* 241: 173–177.

41 Yang, Y., Zhang, Y., Liu, T. et al. (2019). Improved broad temperature adaptability and energy density of vanadium redox flow battery based on sulfate-chloride mixed acid by optimizing the concentration of electrolyte. *J. Power Sources* 415: 62–68.

42 Mousa, A. and Skyllas-Kazacos, M. (2015). Effect of additives on the low-temperature stability of vanadium redox flow battery negative half-cell electrolyte. *ChemElectroChem* 2: 1742–1751.

43 Peng, S., Wang, N.-F., Wu, X.-J. et al. (2012). Vanadium species in CH_3SO_3H and H_2SO_4 mixed acid as the supporting electrolyte for vanadium redox flow battery. *Int. J. Electrochem. Sci.* 7: 643–649.

44 Skyllas-Kazacos, M., Peng, C., and Cheng, M. (1999). Evaluation of precipitation inhibitors for supersaturated vanadyl electrolytes for the vanadium redox battery. *Electrochem. Solid-State Lett.* 2: 121–122.

45 Roe, S., Menictas, C., and Skyllas-Kazacos, M. (2016). The effect of additives on the high-temperature stability of the vanadium redox flow battery positive electrolytes. *J. Electrochem. Soc.* 163: A5023–A5028.

46 Kausar, N., Mousa, A., and Skyllas-Kazacos, M. (2016). A high energy density vanadium redox flow battery with 3 M vanadium electrolyte. *ChemElectroChem* 3: 276–282.

47 Flox, C., Rubio-Garcia, J., Skoumal, M. et al. (2015). Thermally stable positive electrolytes with a superior performance in all-vanadium redox flow batteries. *ChemPlusChem* 80: 354–358.

48 Li, S., Huang, K., Liu, S. et al. (2011). Effect of organic additives on positive electrolyte for vanadium redox battery. *Electrochim. Acta* 56: 5483–5487.

49 Wu, X., Liu, S., Wang, N. et al. (2012). Influence of organic additives on electrochemical properties of the positive electrolyte for all-vanadium redox flow battery. *Electrochim. Acta* 78: 475–482.

50 Chen, R., Henkensmeier, D., Kim, S. et al. (2018). Improved all-vanadium redox flow batteries using catholyte additive and a cross-linked methylated polybenzimidazole membrane. *ACS Appl. Energy Mater.* 1: 6047–6055.

51 Xi, J., Wu, Z., Teng, X. et al. (2008). Self-assembled polyelectrolyte multilayer modified Nafion membrane with suppressed vanadium ion crossover for vanadium redox flow batteries. *J. Mater. Chem.* 18: 1232–1238.

52 Ressel, S., Billa, F., Holtz, L. et al. (2018). State of charge monitoring of vanadium redox flow batteries using half cell potentials and electrolyte density. *J. Power Sources* 378: 776–783.

53 Huheey, J.E., Keiter, E.A., and Keiter, R.L. (2014). *Anorganische Chemie: Prinzipien von Struktur und Reaktivität*, 579–580. Berlin/Boston: Walter de Gruyter GmbH.

54 Geiser, J., Natter, H., Hempelmann, R. et al. (2019). Photometrical determination of the state-of-charge in vanadium redox flow batteries part I: in combination with potentiometric titration. *Z. Phys. Chem.* doi: 10.1515/zpch-2019-1379.

55 Geiser, J., Natter, H., Hempelmann, R. et al. (2019). Photometrical determination of the state-of-charge in vanadium redox flow batteries part II: in combination with open-circuit-voltage. *Z. Phys. Chem.* doi: 10.1515/zpch-2019-1380.

56 Sun, C., Chen, J., Zhang, H. et al. (2010). Investigations on transfer of water and vanadium ions across Nafion membrane in an operating vanadium redox flow battery. *J. Power Sources* 195: 890–897.

57 Yoshitake, M. and Watakabe, A. (2008). *Advances in Polymer Science, Perfluorinated Ionic Polymers for PEFCs*, vol. 215, 127–155. Springer.

58 Oldenburg, F.J., Nilsson, E., Schmidt, T.J. et al. (2019). Tackling capacity fading in vanadium redox flow batteries with amphoteric polybenzimidazole/nafion bilayer membranes. *ChemSusChem* 12: 2620–2627.

59 Noh, C., Jung, M., Henkensmeier, D. et al. (2017). Vanadium redox flow batteries using meta-polybenzimidazole-based membranes of different thicknesses. *ACS Appl. Mater. Interfaces* 9: 36799–36809.

60 Semiz, L., Sankir, N.D., and Sankir, M. (2014). Directly copolymerized disulfonated poly(arylene ether sulfone) membranes for vanadium redox flow batteries. *Int. J. Electrochem. Sci.* 9: 3060–3067.

61 Chen, D., Hickner, M.A., Agar, E. et al. (2013). Optimized anion exchange membranes for vanadium redox flow batteries. *ACS Appl. Mater. Interfaces* 5: 7559–7566.

62 Lee, Y., Kim, S., Maljusch, A. et al. (2019). Polybenzimidazole membranes functionalised with 1-methyl-2-mesitylbenzimidazolium ions via a hexyl linker for use in vanadium flow batteries. *Polymer* 174: 210–217.

63 Choi, N.H., Kwon, S.-k., and Kim, H. (2013). Analysis of the oxidation of the V(II) by dissolved oxygen using UV-visible spectrophotometry in a vanadium redox flow battery. *J. Electrochem. Soc.* 160: A973–A979.

64 Brooker, R.P., Bell, C.J., Bonville, L.J. et al. (2015). Determining vanadium concentrations using the UV-vis response method. *J. Electrochem. Soc.* 162: A608–A613.

65 Jung, M., Lee, W., Noh, C. et al. (2019). Blending polybenzimidazole with an anion exchange polymer increases the efficiency of vanadium redox flow batteries. *J. Membr. Sci.* 580: 110–116.

66 Wang, H. and Turner, J.A. (2008). The influence of metal ions on the conductivity of Nafion 112 in polymer electrolyte membrane fuel cell. *J. Power Sources* 183: 576–580.

67 Wang, L., Pingitore, A.T., Xie, W. et al. (2019). Sulfonated PBI gel membranes for redox flow batteries. *J. Electrochem. Soc.* 166: A1449–A1455.

68 Schwenzer, B., Zhang, J., Kim, S. et al. (2011). Membrane development for vanadium redox flow batteries. *ChemSusChem* 4: 1388–1406.

69 Yuan, Z., Li, X., Zhao, Y. et al. (2015). Mechanism of polysulfone-based anion exchange membranes degradation in vanadium flow battery. *ACS Appl. Mater. Interfaces* 7: 19446–19454.

70 Jeong, S., Kim, L.-H., Kwon, Y. et al. (2014). Effect of Nafion membrane thickness on performance of vanadium redox flow battery. *Korean J. Chem. Eng.* 31: 2081–2087.

71 Jiang, B., Wu, L., Yu, L. et al. (2016). A comparative study of Nafion series membranes for vanadium redox flow batteries. *J. Membr. Sci.* 510: 18–26.

72 Jiang, B., Yu, L., Wu, L. et al. (2016). Insights into the impact of the Nafion membrane pretreatment process on vanadium flow battery performance. *ACS Appl. Mater. Interfaces* 8: 12228–12238.

73 Vijayakumar, M., Luo, Q., Lloyd, R. et al. (2016). Tuning the perfluorosulfonic acid membrane morphology for vanadium redox-flow batteries. *ACS Appl. Mater. Interfaces* 8: 34327–34334.

74 Kreuer, K.D. (2001). On the development of proton conducting polymer membranes for hydrogen and methanol fuel cells. *J. Membr. Sci.* 185: 29–39.

75 Kim, S., Tighe, T.B., Schwenzer, B. et al. (2011). Chemical and mechanical degradation of sulfonated poly(sulfone) membranes in vanadium redox flow batteries. *J. Appl. Electrochem.* 41: 1201–1213.

76 Kamcev, J., Paul, D.R., and Freeman, B.D. (2015). Ion activity coefficients in ion exchange polymers: applicability of manning's counterion condensation theory. *Macromolecules* 48: 8011–8024.

77 Mai, Z., Zhang, H., Zhang, H. et al. (2013). Anion-conductive membranes with ultralow vanadium permeability and excellent performance in vanadium flow batteries. *ChemSusChem* 6: 328–335.

78 Coury, L. (1999). Conductance measurements part 1: theory. *Curr. Sep.* 18: 91–96.

79 Koros, W.J., Ma, Y.H., and Shimidzu, T. (1996). Terminology for membranes and membrane processes. *J. Membr. Sci.* 120: 149–159.

80 Liu, Z., Li, R., Chen, J. et al. (2017). Theoretical investigation into suitable pore sizes of membranes for vanadium redox flow batteries. *ChemElectroChem* 4: 2184–2189.

81 Hsu, W.Y. and Gierke, T.D. (1983). Ion transport and clustering in Nafion perfluorinated membranes. *J. Membr. Sci.* 13: 307–326.

82 Chae, I.S., Luo, T., Moon, G.H. et al. (2016). Ultra-high proton/vanadium selectivity for hydrophobic polymer membranes with intrinsic nanopores for redox flow battery. *Adv. Energy Mater.* 6: 1600517.

83 Zhang, H., Zhang, H., and Li, X. (2013). Nanofiltration membranes for vanadium flow battery application. *ECS Trans.* 53: 65–68.

84 Zhang, H., Zhang, H., Li, X. et al. (2011). Nanofiltration (NF) membranes: the next generation separators for all vanadium redox flow batteries (VRBs)? *Energy Environ. Sci.* 4: 1676.

85 Zhou, X.L., Zhao, T.S., An, L. et al. (2015). The use of polybenzimidazole membranes in vanadium redox flow batteries leading to increased coulombic efficiency and cycling performance. *Electrochim. Acta* 153: 492–498.

86 Yuan, Z., Duan, Y., Zhang, H. et al. (2016). Advanced porous membranes with ultra-high selectivity and stability for vanadium flow batteries. *Energy Environ. Sci.* 9: 441–447.

87 Lee, W., Jung, M., Serhiichuk, D. et al. (2019). Layered composite membranes based on porous PVDF coated with a thin, dense PBI layer for vanadium redox flow batteries. *J. Membr. Sci.* 591: 117333.

88 Jung, M., Lee, W., Krishnan, N.N. et al. (2018). Porous-Nafion/PBI composite membranes and Nafion/PBI blend membranes for vanadium redox flow batteries. *Appl. Surf. Sci.* 450: 301–311.

89 Peng, S., Yan, X., Zhang, D. et al. (2016). A H_3PO_4 preswelling strategy to enhance the proton conductivity of a H_2SO_4-doped polybenzimidazole membrane for vanadium flow batteries. *RSC Adv.* 6: 23479–23488.

90 Jang, J.-K., Kim, T.-H., Yoon, S.J. et al. (2016). Highly proton conductive, dense polybenzimidazole membranes with low permeability to vanadium and enhanced H_2SO_4 absorption capability for use in vanadium redox flow batteries. *J. Mater. Chem. A* 4: 14342–14355.

91 Wei, H., Liu, Y., Xu, W. et al. (2019). Polyethylene/PBI pore-filling composite membrane for high performance vanadium redox flow battery. *J. Electrochem. Soc.* 166: A3207–A3209.

92 Chromik, A., dos Santos, A.R., Turek, T. et al. (2015). Stability of acid-excess acid–base blend membranes in all-vanadium redox-flow batteries. *J. Membr. Sci.* 476: 148–155.

93 Krishnan, N.N., Henkensmeier, D., Jang, J.H. et al. (2014). Nanocomposite membranes for polymer electrolyte fuel cells. *Macromol. Mater. Eng.* 299: 1031–1041.

94 Leung, P.K., Xu, Q., Zhao, T.S. et al. (2013). Preparation of silica nanocomposite anion-exchange membranes with low vanadium-ion crossover for vanadium redox flow batteries. *Electrochim. Acta* 105: 584–592.

95 Ahn, S.M., Jeong, H.Y., Jang, J.-K. et al. (2018). Polybenzimidazole/Nafion hybrid membrane with improved chemical stability for vanadium redox flow battery application. *RSC Adv.* 8: 25304–25312.

96 Chen, R., Trieu, V., Schley, B. et al. (2013). Anodic electrocatalytic coatings for electrolytic chlorine production: a review. *Z. Phys. Chem.* 227: 651–666.

97 Kim, K.J., Park, M.-S., Kim, Y.-J. et al. (2015). Application of carbon materials in redox flow batteries. *J. Mater. Chem. A* 3: 16913–16933.

98 Chakrabarti, M.H., Brandon, N.P., Hajimolana, S.A. et al. (2014). A technology review of electrodes and reaction mechanisms in vanadium redox flow batteries. *J. Power Sources* 253: 150–166.

99 Melke, J., Jakes, P., Langner, J. et al. (2014). Carbon materials for the positive electrode in all-vanadium redox flow batteries. *Carbon* 78: 220–230.

100 Zhong, S., Padeste, C., Kazacos, M. et al. (1993). Comparison of the physical, chemical and electrochemical properties of rayon- and polyacrylonitrile-based graphite felt electrodes. *J. Power Sources* 45: 29–41.

101 Sun, B. and Skyllas-Kazacos, M. (1992). Modification of graphite electrode materials for vanadium redox flow battery application – I. Thermal treatment. *Electrochim. Acta* 37: 1253–1260.

102 Sun, B. and Skyllas-Kazacos, M. (1992). Chemical modification of graphite electrode materials for vanadium redox flow battery application – part II. Acid treatments. *Electrochim. Acta* 37: 2459–2465.

103 Zhang, W., Xi, J., Li, Z. et al. (2013). Electrochemical activation of graphite felt electrode for VO^{2+}/VO_2^+ redox couple application. *Electrochim. Acta* 89: 429–435.

104 Zhou, H., Xi, J., Li, Z. et al. (2014). Graphite–graphite oxide composite electrode for vanadium redox flow battery. *RSC Adv.* 4: 61912–61918.

105 Li, W., Liu, J., and Yan, C. (2011). High performance electrodes in vanadium redox flow batteries through oxygen-enriched thermal activation. *Electrochim. Acta* 56: 5290–5294.

106 Pezeshki, A.M., Clement, J.T., Veith, G.M. et al. (2015). Redox flow batteries: a review. *J. Power Sources* 294: 333–338.

107 Weber, A.Z., Mench, M.M., Meyers, J.P. et al. (2011). Nitrogen-doped mesoporous carbon for energy storage in vanadium redox flow batteries. *J. Appl. Electrochem.* 41: 1137–1164.

108 Shao, Y., Wang, X., Engelhard, M. et al. (2010). CeO_2 decorated graphite felt as a high-performance electrode for vanadium redox flow batteries. *J. Power Sources* 195: 4375–4379.

109 Wei, G., Jia, C., Liu, J. et al. (2012). Carbon felt supported carbon nanotubes catalysts composite electrode for vanadium redox flow battery application. *J. Power Sources* 220: 185–192.

110 Chen, R., Kim, S., and Chang, Z. (2017). Redox flow batteries: fundamentals and applications. In: *Redox – Principles and Advanced Applications* (ed. M.A.A. Khalid), 103–118. London: IntechOpen.

111 Aaron, D.S., Liu, Q., Tang, Z. et al. (2012). Dramatic performance gains in vanadium redox flow batteries through modified cell architecture. *J. Power Sources* 206: 450–453.

112 Darling, R.M. and Perry, M.L. (2014). The influence of electrode and channel configurations on flow battery performance. *J. Electrochem. Soc.* 161: A1381–A1387.

113 Ma, X., Zhang, H., Sun, C. et al. (2012). An optimal strategy of electrolyte flow rate for vanadium redox flow battery. *J. Power Sources* 203: 153–158.

114 Kim, D.K., Yoon, S.J., Lee, J. et al. (2018). Parametric study and flow rate optimization of all-vanadium redox flow batteries. *Appl. Energy* 228: 891–901.

115 Yoon, S.J., Kim, S., and Kim, D.K. (2019). Optimization of local porosity in the electrode as an advanced channel for all-vanadium redox flow battery. *Energy* 172: 26–35.

116 Yin, C., Gao, Y., Guo, S. et al. (2014). A coupled three dimensional model of vanadium redox flow battery for flow field designs. *Energy* 74: 886–895.

117 Tang, A., Bao, J., and Skyllas-Kazacos, M. (2014). Studies on pressure losses and flow rate optimization in vanadium redox flow battery. *J. Power Sources* 248: 154–162.

118 Xu, Q., Zhao, T.S., and Leung, P.K. (2013). Numerical investigations of flow field designs for vanadium redox flow batteries. *Appl. Energy* 105: 47–56.

119 Derr, I., Przyrembel, D., Schweer, J. et al. (2017). Electroless chemical aging of carbon felt electrodes for the all-vanadium redox flow battery (VRFB) investigated by Electrochemical Impedance and X-ray Photoelectron Spectroscopy. *Elctrochim. Acta* 246: 783–793.
120 Schneider, J., Bulczak, E., El-Nagar, G.A. et al. (2019). Degradation phenomena of bismuth-modified felt electrodes in VRFB studied by electrochemical impedance spectroscopy. *Batteries* 5: 16.
121 Derr, I., Bruns, M., Langner, J. et al. (2016). Degradation of all-vanadium redox flow batteries (VRFB) investigated by electrochemical impedance and X-ray photoelectron spectroscopy: Part 2 electrochemical degradation. *J. Power Sources* 325: 351–359.
122 Derr, I., Fetyan, A., Schutjajew, K. et al. (2017). Electrochemical analysis of the performance loss in all vanadium redox flow batteries using different cut-off voltages. *Electrochim. Acta* 224: 9–16.